Tunable magnetic and magnetotransport properties in locally epitaxial $La_{0.67}Sr_{0.33}MnO_3$ thin films on polycrystalline $SrTiO_3$, by control of grain size.

Marie Dallocchio[1], Alexis Boileau[1], Bernard Mercey[1], Adrian David[1], Ulrike Lüders[1], Sandrine Froissart[1], Xavier Larose[1], Bruno Bérini[2], Yves Dumont[2], Alain Pautrat[1], Wilfrid Prellier[1], Arnaud Fouchet[1*].

[1] NORMANDIE UNIV, ENSICAEN, UNICAEN, CNRS, CRISMAT, 14000 CAEN, FRANCE.
[2] Groupe d'Etude de la Matière Condensée (GEMaC), Université Paris-Saclay, UMR 8635 Université de Versailles Saint-Quentin en Yvelines & CNRS, Versailles, France

* Corresponding author:
E-mail: arnaud.fouchet@ensicaen.fr

Abstract:

$La_{0.67}Sr_{0.33}MnO_3$ (LSMO) thin films have been grown by pulsed laser deposition on $SrTiO_3$ using combinatorial substrate epitaxy (CSE) approach, i.e. polycrystalline substrates with micrometer-size grains. The crystallographic domains size of those polycrystalline substrates can be controlled between 2 to 45 µm depending on the annealing temperature during synthesis. Each grain of the substrate acts as a single crystalline growth template promoting local epitaxy with a reproduction of the substrate grain structure in the thin film. Therefore, a fine-tuning of the substrate grain metrics and high crystalline quality of locally epitaxial LSMO film, allows to combine the advantages of polycrystalline, i.e. the presence of low field magnetoresistance (LFMR) and the possibility to use very thin films, with a pronounced magnetic shape anisotropy. For this, the magnetic and transport properties of the films are showing a strong influence with varying grain metrics of the substrate. High Curie temperatures, important values of the LFMR and anisotropy for optimized substrate grain metrics with the relative orientation of the magnetic field to the film plane underline the high quality of the films and the advantage of the CSE approach. The obtained LSMO thin films may have an interest for high-resolution low field magnetic sensors application.

Keywords: Thin films, LSMO, polycrystalline substrates, EBSD, physical properties, LFMR, CMR.

1. Introduction

Complex oxides are a broad family of materials presenting various unique physical effects such as a wide range of magnetic phases, strongly correlated transport and even superconductivity [1–3]. Among this family, mixed valence manganites crystallizing with the perovskite structure $RE_{1-x}M_xMnO_3$ (with RE: rare earth and M: alkaline earth) present a high magnetoresistance and half-metallic properties, making this material interesting for potential applications in magnetic field sensing or spintronic devices [4–7]. By varying the composition between RE and M, complex phase diagrams are observed illustrating the high tunability of the magnetic and the transport properties of the manganites [8]. In the case of $La_{1-x}Sr_xMnO_3$ (LSMO) with x = 0.33, a ferromagnetic, half-metallic phase is observed up to the Curie temperature (T_C) of 370 K [9]. Due to the double exchange (DE) interaction of the mixed valence Mn ions, the magnetic transition at T_C is associated to a metal insulator transition, leading to the colossal magnetoresistance effect (CMR) [8–13]. Furthermore, in polycrystalline materials [14,15], new properties can emerge, such as low field magnetoresistance (LFMR) interesting for low field magnetic sensors [16,17], as a result of spin-dependent tunneling through grain boundaries [18]. LFMR is thus strongly influenced by the grain boundary density and the size of the crystallographic domains. One of the most efficient techniques to control the LFMR is the nanostructuration of the LSMO film by nanocomposite approach [19,20]. Nevertheless, this approach requires to use specific material systems, those who allow for the spontaneous demixing during the deposition process, with eventual negative effects on the LFMR and the quality of the LSMO phase.

An interesting alternative to gain external control on the grain structure of the LSMO films and therefore the LFMR, is to use the combinatorial substrate epitaxy (CSE) approach. In this approach, the substrate is a sintered polycrystalline, mirror polished ceramic [21], exhibiting different crystallographic orientations at its surface. Each grain at the surface can be considered as a local single-crystalline growth template, and for high deposition temperatures, an epitaxial grain-on-grain growth of the thin film, can be achieved. While in classical synthesis routes used for deposition of polycrystalline films, the grain size is driven by the density of nucleation sites and the thermodynamic imposed by the deposition or post-annealing conditions; in the CSE approach, the epitaxial grain-on-grain growth leads to a transfer of the grain metrics from the substrate to the thin film. Several types of CSE substrates have already been developed including the rhombohedral compound Al_2O_3 [22,23] and the perovskite-type substrates $LaAlO_3$ (LAO) [24] and $SrTiO_3$ (STO) [25]. Interestingly, for STO, it was also shown that on each grain, atomically flat surfaces can be obtained, favoring a high quality thin film growth. Moreover, CSE provides new possibilities to obtain exotic phases, such as layered perovskite $La_2Ti_2O_7$, as substrate to promote the growth of pyrochlore phase [26]; or the growth of Ruddlesden-Popper phase (RPP) on isostructural substrates [27]. A significant advantage is also their production cost, which is much lower compared to single-crystal substrates. Indeed, these last ones require slow and expensive growth techniques, while in the CSE approach, we use standard and fast ceramics synthesis techniques as spark plasma

sintering (SPS). But even more, CSE opens the possibility to enhance some functional physical properties by the introduction of grain boundaries. This kind of defects with long-range translational symmetry breaking can be interesting particularly for thermoelectric properties [28].

In this context, we will show that the CSE approach can also be interesting to control the grain size and therefore the density of grain boundaries in order to control the physical properties of LSMO films deposited on polycrystalline substrates. The grain metrics of the thin film is therefore directly related to the annealing process of the substrate ceramics, allowing for a larger variation of the grain sizes and the grain boundary density. By the use of different annealing temperatures during the SPS process, we are able to tune the substrate grain sizes from 2 to 45 µm.

The present work aims to investigate the impact of the substrate grain metrics on the properties of the CSE LSMO thin films, combining an in-depth study of the microstructure of the films, their magnetic properties, their transport properties and the magnetotransport. As in all cases, the same deposition conditions of the LSMO films were used, the impact of post-annealing treatments usually used to synthesize polycrystalline films on their properties can be avoided in this study, allowing to single out the effect of the change of grain metrics.

2. Experimental Section

All polycrystalline $SrTiO_3$ substrates were synthesized by spark plasma sintering (SPS), starting from the two precursors TiO_2 (Cerac,99.5% purity) and $SrCO_3$ (Aldrich, 99.9% purity). The powder was mixed with an attritor for 2 h with ethanol, using small ZrO_2 balls, dried afterwards with an IR lamp and grinded manually with a mortar and pestle. A first calcination annealing at 1200 °C for 12 hours is followed by another mechanical grinding step during 16 min in order to eliminate agglomerates.

Once the $SrTiO_3$ powder is obtained, 4 g is introduced into a 20 mm diameter mold covered with Papyex (graphite). For the SPS sintering, the temperature annealing is reached at 100 °C/min with a pressure of 7 kN. Then a pressure of uniaxial force of 16 kN is applied to the sample for 20 min at the desired temperature (i.e. 1200 °C, 1300 °C, 1400 °C and 1500 °C). Then a ramp of 100 °C/min is applied until room temperature with a 7 kN. Finally, a 2 cm diameter pellets is obtained.

Afterward, the sintered pellets have been cut and polished in order to obtain flat surfaces required for the film deposition and EBSD analysis. The polishing process begins manually by several SiC papers decreasing successively the grain size (30, 15, 10 and 5 µm) and finishes automatically using a Struers polisher with diamond liquid pastes (3 µm and 1µm). Finally, the samples are polished with a Si-colloidal solution, in order to obtain a mirror-like surface [25,27].

$La_{0.67}Sr_{0.33}MnO_3$ (LSMO) thin films of 40 nm have been grown on polycrystalline mirror-

polished CSE substrates and on (001)-oriented $SrTiO_3$ substrates by pulsed laser deposition (PLD) [29]. The depositions were carried out at 645 °C under oxygen-ozone mixture conditions [29,30], with a partial pressure of 6.4E-4 mbar. A KrF excimer laser (λ= 248 nm) was used with a repetition rate of 2 Hz and a deposition rate close to 0.1 Å per laser pulse.

The LSMO target were synthetized by solid solution in a conventional oven. The starting materials were $SrCO_3$ (99% purity), La_2O_3 (99.9% purity) and MnO_2 (99.99% purity) which were ground together in a mortar and pestle. The ground materials were calcined at 1000 °C in air for 4 hours. The polycrystalline material was then re-ground, mixed with rhodoviol (polyvinyle alcool) and pressed into a pellet (1 inch diameter). It was finally sintered at 1350°C in air for 4 hours before being used as a target.

The morphology of the surface was characterized by an atomic force microscopy (AFM, Bruker Icon) in PeakForce tapping mode with ScanAsyst-Air tip. The local structure was investigated by scanning electron microscope (SEM) and electron backscatter diffraction (EBSD, with Zeiss Supra 55). The conditions for EBSD acquisition were accelerating voltage = 15 kV, diaphragm aperture = 60 μm and working distance = 15 mm. LSMO on polycristalline STO films were also investigated by grazing incidence X-ray diffraction (GIXRD), (see figure S6).

Magnetization measurements were performed using a superconducting Quantum Interference Devices, the SQUID MPMS XL, with the field applied parallel and perpendicular to the film plane. All M(T) and M(H) curves presented are raw data. The M(T) was measured with a magnetic field of 0.005 T around the magnetic transition after applying a field of 1 T at low temperature. Magnetoresistance and resistivity measurements were realized by four-point method using a physical properties measurement system (PPMS) with magnetic field applied parallel and perpendicular to the film surface.

3. Results and discussion

3.1 Structural analyses

The influence of the sintering temperature (from 1200 to 1500 °C) of the STO polycrystalline substrates is investigated by electron backscatter diffraction (EBSD) mapping and reported in figure 1(a-d). The color gradient of the individual grains shows their relative orientations with respect to the [100], [101] and [111] directions, as indicated by the stereographic unit triangle (see figure 1f). The uniform distribution of the different colors in the EBSD maps indicates the absence of any crystallographic texture, thus, all crystalline orientations are present in the different substrates.

The distribution of the grain size was extracted from figures 1(a-d) and summarized in figure 1e, where a large variation of the average grain size with the sintering temperature is observed. The lowest sintering temperature (1200 °C) induces a narrowed distribution consisting

of small grain size (average size of 2 µm). At higher sintering temperatures, a bimodal character of the distribution can be observed. In spite of this bimodal distribution, the overall range of grain sizes is different for all samples, and the average grain sizes differ from 2 to 45 µm.

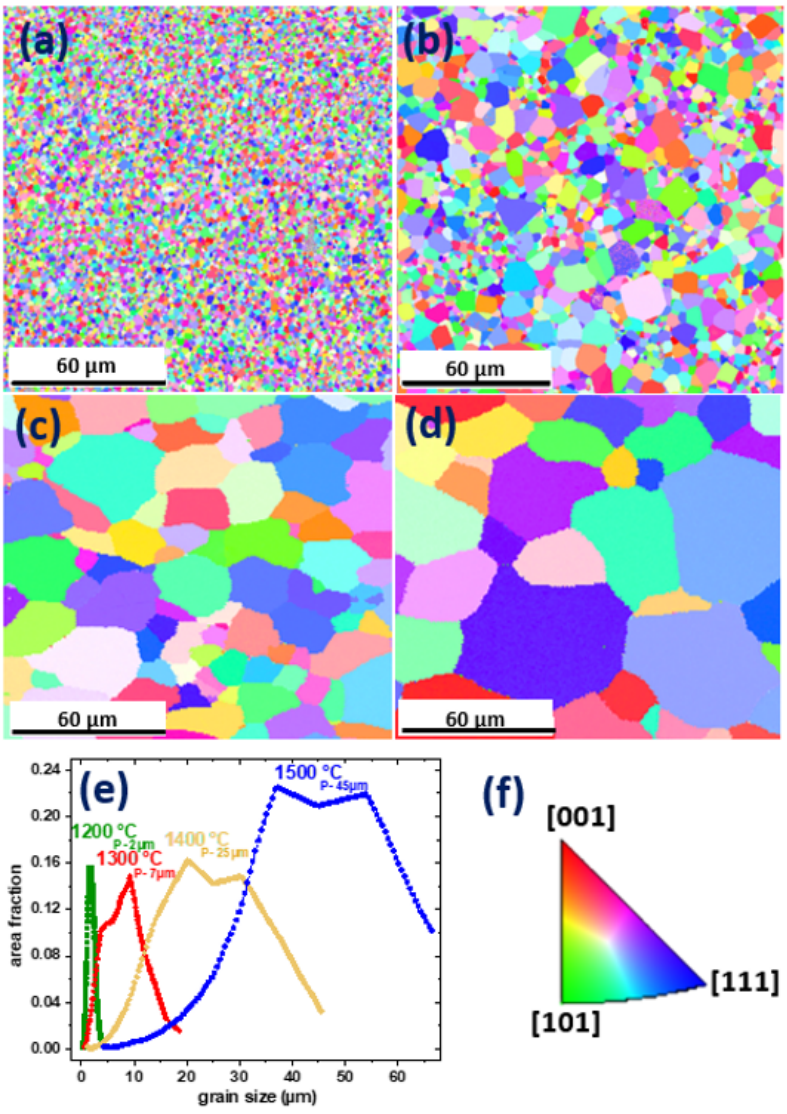

Figure 1. EBSD mappings of STO polycrystalline substrates with different grain sizes for different sintering temperatures: 1200 °C (a), 1300 °C (b), 1400 °C (c), 1500 °C (d). In (e) is summarized the average grain size versus sintering temperature; For (c) and (d), areas chosen were higher than (a) and (b), to respect grain statistic. In (f), stereographic unit triangle is presented for the cubic phase of the EBSD mapping.

After deposition of LSMO thin films on the polycrystalline substrate, EBSD measurements were again performed in the same area in order to study the orientation relationship between the films and the polycrystalline substrate. Figure 2 presents EBSD mapping of the pristine substrate (45 µm grain size) and the same area after deposition of LSMO. For the analysis of the EBSD maps, different crystallographic phases between STO and LSMO were used for the determination of the grain orientation (cubic phase: $Pm\bar{3}m$ for STO and quadratic phase: $I4/mmm$ for LSMO). Since the shape and the color of each grain are similar in both images, we conclude to a cube on cube epitaxial growth on each individual grain. This coherent growth is observed for all the substrates with different domain sizes, which is in perfect agreement with previous studies for this film thickness [18,27,31].

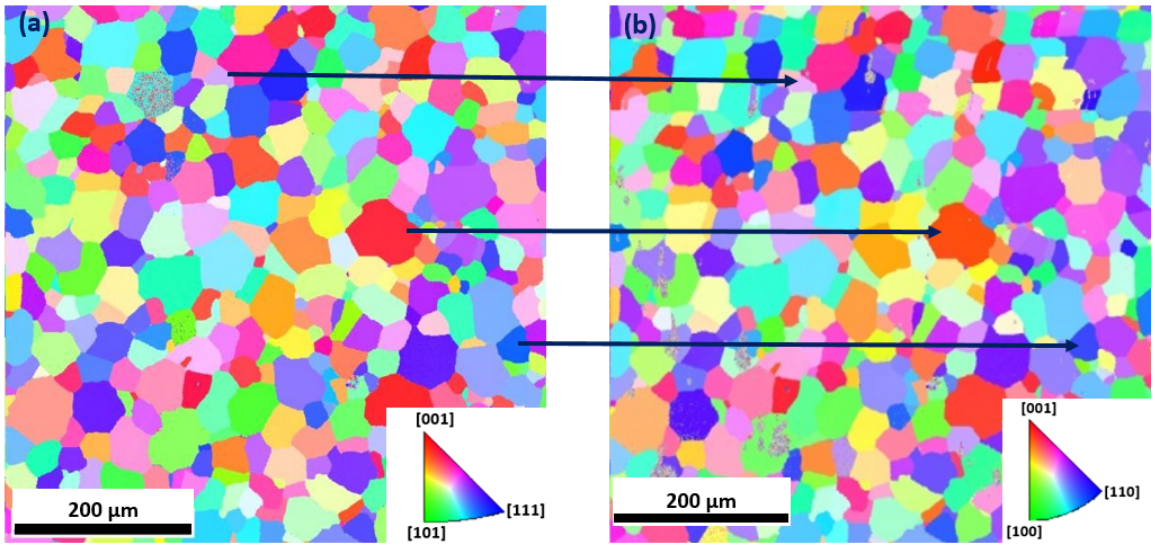

Figure 2. EBSD mappings of the 45 µm grain size substrate without (a) and with (b) LSMO thin film. The stereographic unit triangle for cubic (a) or quadratic (b) phase is shown in insets.

The surface morphologies of the films were also investigated by AFM (see figure 3). Contrariwise to the EBSD micrographs, all the grains are observable even for the 2 µm grain size. The observed grains are well defined and present a relatively smooth surface. A zoom shows the grain boundaries with a small gap between adjacent grains. The analysis of the intergrain area shows a width of 7 to 40 nm (see on figure S1) with a depth of 5 nm. Furthermore, small nanostructures of a 4-7 nm height size appear in the grain area, depending on the orientation of each grain. The root means square (RMS) roughness value of each grain is around 2-3 nm, which indicates a smooth growth of the film on each grain. Moreover, at this scale some porosities between the grains can be observed on figure 3b which probably result from the sintering process. Similar observations have been obtained on the films with 45 µm grain size (figure 3c and d).

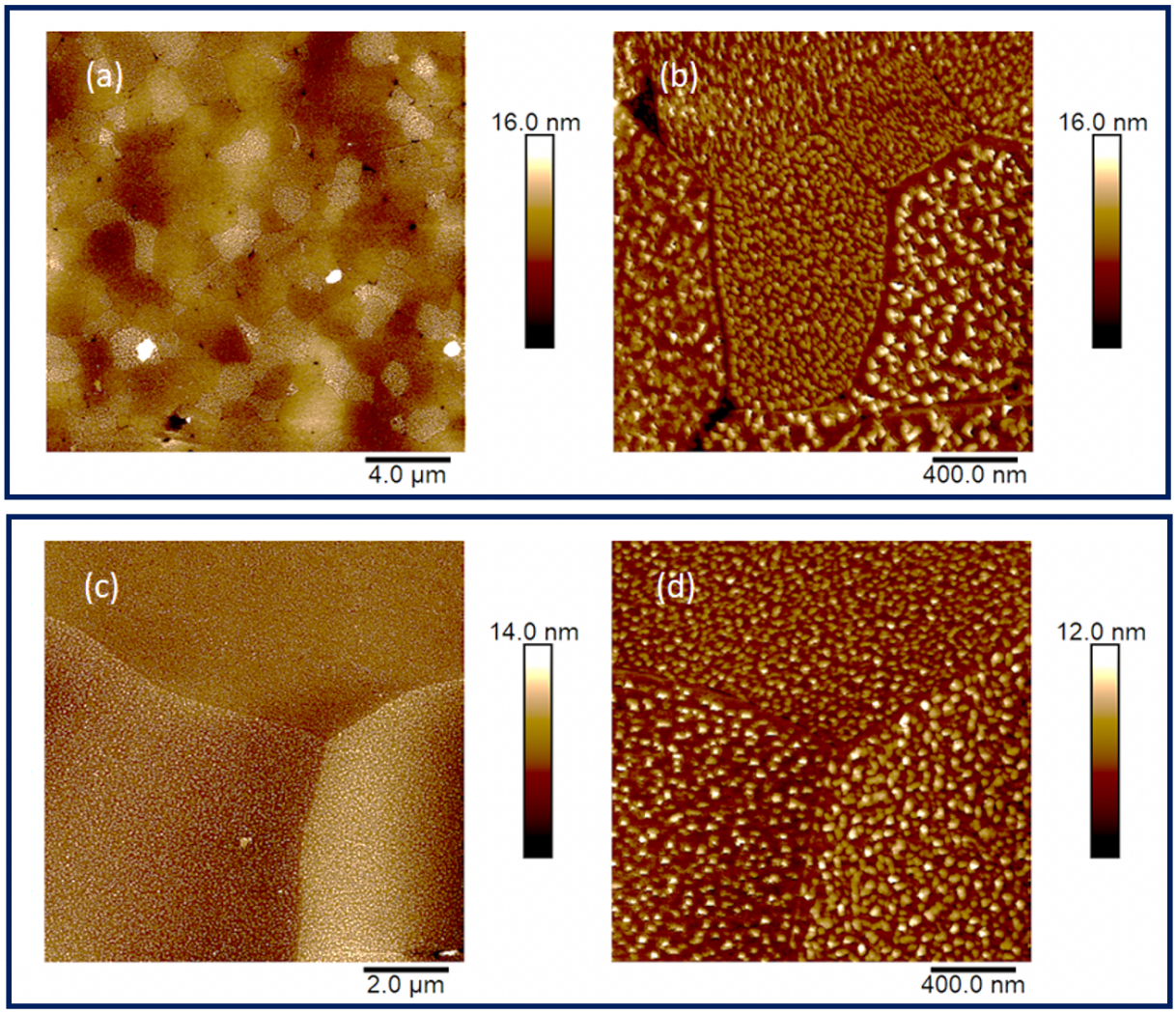

Figure 3. AFM mappings of LSMO polycrystalline films with grain size of 2 µm (a and b) and with grain size of 45 µm (c and d).

3.2 Magnetic properties

The variation of magnetization versus temperature of the LSMO films grown on the different polycrystalline substrates is shown in figure 4a. By comparison, LSMO on STO single-crystal (LSMO-SC) is also presented and shows a Curie temperature (T_C) of 332 K (for more details about the T_C determination, the first derivative of the magnetization curves (dM/dT) is also presented in figure S2). Therefore the T_C value of the LSMO thin film grown on STO is in perfect agreement with the literature [30,32]. Nevertheless, compared to the bulk LSMO where the reported T_C value is around 370 K, we observe a decrease of the magnetic transition temperature, which is due to the tensile strain (lattice mismatch = -1.15 %) imposed by the single-crystal STO

substrates to the LSMO film [33,34]. The T_C decrease can be related to the distortion of the LSMO structure corresponding to the tilting of O-Mn-O bonds angle and O-Mn bond length [35,36] induced by the tensile strain. All LSMO films on polycrystalline substrates show a higher T_C, in the range of 353 K (figure 4a), approaching the bulk value of 370 K. Comparable T_C values (see in table 1) have been also observed in other polycrystalline films [18,19,34,37,38], with values between those of single-crystal thin films and those of the bulk. It is interesting to note, that out-of-plane textured LSMO films [34] show T_C values of about 340 K, only slightly higher than the single-crystal films [18]. It was shown that the T_C of LSMO is strongly dependent with the different orientations (100), (110) or (111) orientation [39], and strain state of the film with a decrease of the Tc with compressive or tensile strain [29,40,41]. The mixed orientations of LSMO grains in CSE thin films, relaxe the strain at the grains boundries and explain the increase of T_C in CSE compare to single-crystal films. The absence of a T_C dependence on the grain size shows that the presence of the grain boundaries has a negligible effect on T_C, indicating a high crystalline quality of the films.

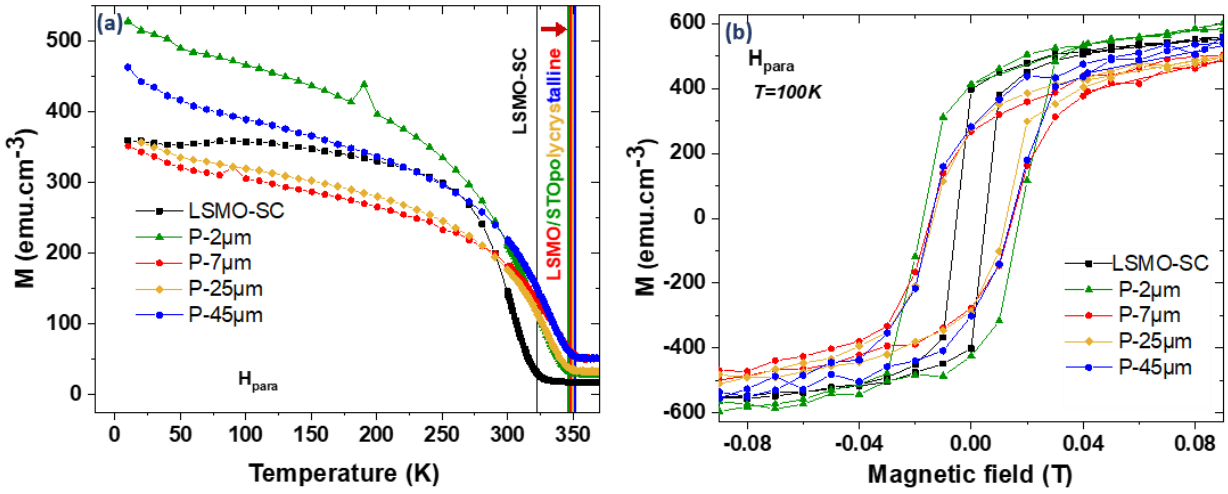

Figure 4. (a) Magnetization versus temperature curve with 0.005 T magnetic field applied parallel to the film surface. (b) Hysteresis loops at 100 K in-plane magnetization with magnetic field applied parallel to the film surface. LSMO on single-crystal STO (LSMO-SC) (black curve) and on polycrystalline STO substrates with different grain sizes: 2 µm, 7µm, 25 µm and 45 µm.

As we can see in figure 4b, the hysteresis loops M(H) present also different behavior between LSMO grown on single-crystal and polycrystalline substrates. Each hysteresis loop was recorded at 100 K with the magnetic field H parallel to the film plane. In all polycrystalline films, the coercive field (H_C = 0.015 T) is higher than in the single-crystal film (H_C = 0.005 T). This increase of coercivity is observed for polycrystalline samples due to the presence of high number

of grain boundaries, which clamp the magnetic domains [18,42] and more energy is needed to return the magnetization.

In the figure S3, the hysteresis loops are shown for a larger magnetic field range. All the polycrystalline films present saturation magnetization (M_S= 600 - 635 emu/cm^3) similar to the single-crystal film, which is in accordance with literature [43] (see also table 1). The value of the magnetization near to the theoretical value, can be explained by the high crystalline quality of the LSMO film. Again, the variation of M_S with the grain size of the films is very small. The grain-on-grain epitaxial growth allows to keep the disorder at the grain boundaries and therefore their influence on the magnetization on a minimum level.

3.3 Magneto-Transport properties

The resistivity and the magnetoresistance of the polycrystalline samples and the single-crystal samples are shown in figure 5. At room temperature, the resistivity (figure 5a) of the single-crystal sample is comparable to the polycrystalline sample with 25 and 45 μm large grains, but at lower temperature, the polycrystalline sample show a smaller decrease of the resistivity, leading to low temperature resistivities being one order of magnitude larger than the value observed for the single-crystal sample. By decreasing the grain size with a critical value below 25 μm, the film resistivity tends to increase as expected due to the increasing perturbation of the electronic transport by the disorder generated in the grain boundaries.

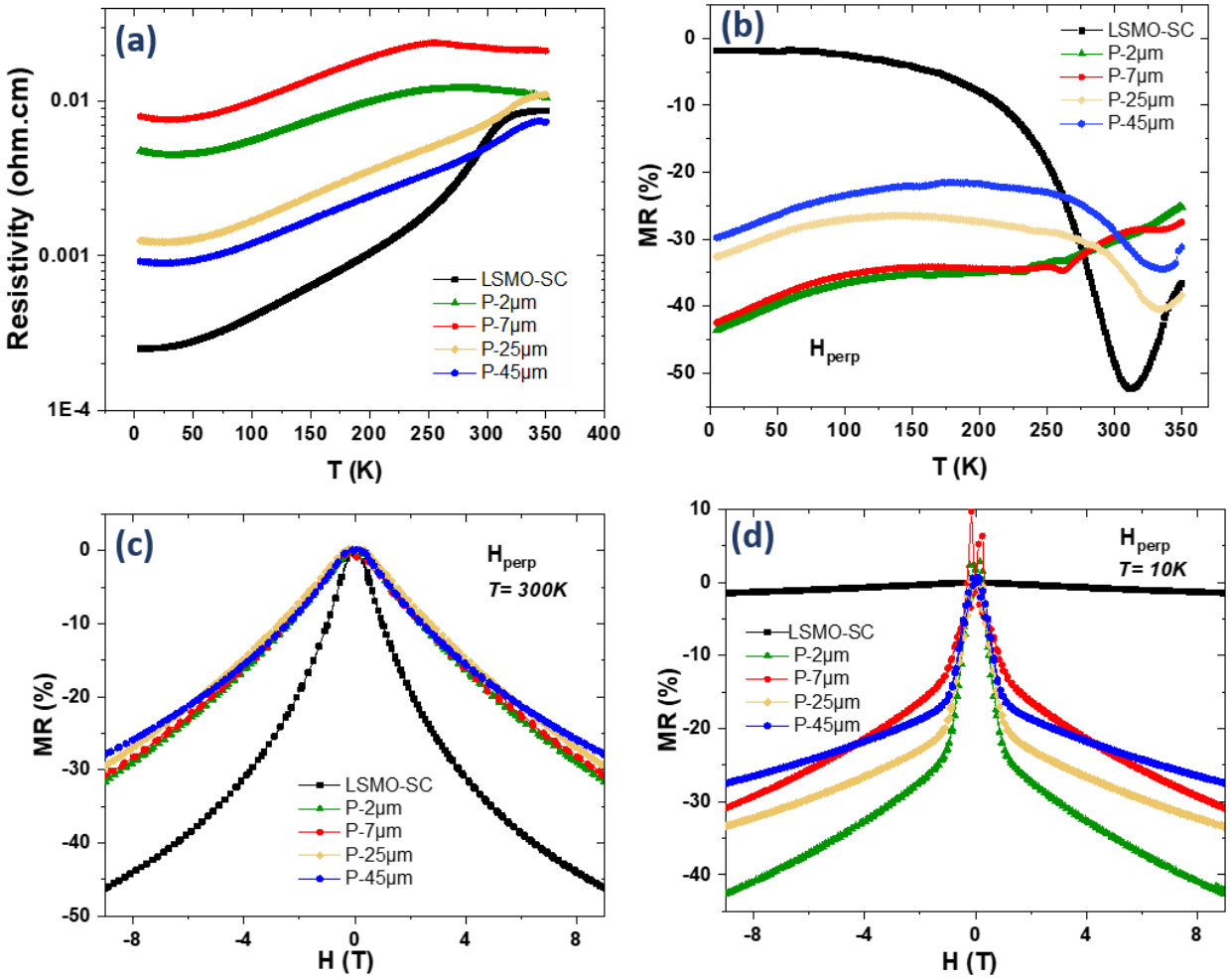

Figure 5. (a) Resistivity (at 0 T) and (b) magnetoresistance measured with magnetic field (9 T) applied perpendicular to the surface at 10 K (d) and 300 K (c) of LSMO films grown on single-crystal STO (black curve) and on polycrystalline STO substrates with different grain sizes: 2 µm, 7 µm, 25 µm and 45 µm.

Figure 5b and S4 depict the temperature dependence of the magnetoresistance (MR). Two contributions to the MR of the polycrystalline films can be identified. The peak around room temperature is due to the CMR effect in LSMO, related to the spin alignment during the magnetic transition (T_P). This MR effect is due to the ordering of the spins at the ferromagnetic transition, leading to a metallic state due to the double-exchange (DE) interactions. In the single-crystal film, this peak is the most intense, and can be equally observed in the CSE films. Nevertheless, with decreasing grain size, the peak is less intense and shifted toward low temperature. For each sample, the discrepancy between T_C (obtained by SQUID measurements) and T_P (obtained by transport), are calculated with $\Delta T = T_C - T_P$ and also summarized in table 1. For the films with grain size of 25 and 45µm, ΔT remains small, but for the samples with the 7 µm or 2 µm grain size, the transport

peak nearly disappears and it shifted to lower temperatures *(*$\Delta T_{2\mu m}$ =86 K). In these samples, the disorder at the grain boundaries is so important that even under a magnetic field, DE chains can only be established at lower temperatures, well below T_C.

A second contribution to the MR of the CSE samples can be observed at lower temperatures. For the single-crystal sample, the MR approaches 0 at low temperatures [18,44], due to the well-established magnetic order, avoiding misaligned spins leading to the CMR effect. In the CSE samples, however, the low temperature MR has a high amplitude in the order of 30-50 %. By recording isothermal MR*(H)* curves (figure 5d) at 10 K, we see the resistivity decreasing rapidly at low magnetic field less than 1.5 T. This behavior is known as low field magnetoresistance (LFMR) [14,15,43,45] and was observed for different type of LSMO thin films from polycrystalline to nanocomposites [15,20,46]. As expected, in the picture of LFMR, the MR increases when the number of grain boundaries increases, thus with decreasing grain sizes. The highest value is found for the 2µm CSE film, reaching -24 % (see table 1) at low temperature. Comparatively to others works, the LFMR value observed for our film is almost the same than obtained for nanocomposite and more precisely for vertically aligned nanocomposites (VAN) thin films: $La_{0.7}Sr_{0.3}MnO_3$:CeO_2 VAN reaches 21 % at 20 K (at H= 1 T) [45] ; and $La_{0.7}Sr_{0.3}MnO_3$:ZnO VAN reaches around -20 % at low temperature (under 1 T) [19,47,48]. Recently, improvements have been made to increase this LFMR with the nanocomposites by inserting a small interlayer between two VAN layers [49] (≈ 37 % around 110 K with H= 1 T).

Nevertheless, our approach consists in depositing a single LSMO layer, providing a simple way of synthesis. Furthermore, as the magnetic properties of the film were only marginally influenced by the grain size, even the 2 µm sample shows still a low coercive field and a high amplitude of the LFMR. Therefore, the CSE approach allows to tune the functional properties of the LSMO films, without detrimental effects related to the crystallization procedure. Especially small grain sizes and good magnetic properties are typically difficult to achieve in post-annealed amorphous films. For small grains, the crystallization process has to be short or at low temperatures, jeopardizing the crystalline quality of the grains and therefore the magnetic properties. If good magnetic properties are achieved, typically, the grain size is large and the grain density is low, decreasing the LFMR. Therefore, the CSE approach allows to get out of this trade-off situation between the grain size and the magnetic properties, and results in small grains with excellent magnetic and therefore magnetoresistive properties.

Table 1. Summarizes all main results of the four polycrystalline films and the single-crystal film, including also related data for similar LSMO film in literature [44,50,51]. With M, ρ, CMR, MR and LFMR respectively the magnetization, resistivity, colossal magnetoresistance, magnetoresistance and low field magnetoresistance.

Ref	Our samples	grain size [µm]	T_c [K]	T_P [K]	$\Delta T=T_c-T_p$ [K]	$\pm M_s$ (1 T) [emu.cm^{-3}]	$\pm H_C$ (100K) [Oe]	ρ_{300K} (0 Oe) [Ω.cm]	CMR (300 K) (to 9 T) [%]	MR (from 1 T to 9 T) (at 10 K) [%]	LFMR (at 10 K) [%]
	LSMO/ STO-SC	-	332	312	20	603; -604	52; -52	5.6×10^{-3}	-46	-	-
	LSMO/polycrystalline (1200°C)	2	355	269	86	635; -634	152; -172	1.3×10^{-2}	-31	-19	-24
	LSMO/polycrystalline (1300°C)	7	353	255	98	618; -614	142; -146	2.2×10^{-2}	-31	-18	-13
	LSMO/polycrystalline (1400°C)	25	353	335	18	612; -611	143; -137	7.2×10^{-3}	-30	-13	-20
	LSMO/polycrystalline (1500°C)	45	354	338	16	619; -618	137; -138	5.1×10^{-3}	-28	-11	-16
[19]	LSMO:ZnO	0.4	300	185			240 (10 K)	10		18.5	<1
[34]	LSMO/ nanosheets/STO-SC	0.40	337	300	37	581; -575	172; -173	2.8×10^{-2}	50		-
[34]	LSMO/glass	0.34	348	257	91	329; -331	357; -357	5.7×10^{-1}	35		-30
[42]	LCMO poly LCMO poly	3 24				~670 ~500	275				
[37]	$La_{0.55}Sr_{0.45}MnOz$	0.1-1.5	320	185							
[52]	polyaniline-manganite Nanocomposites a-b	70 80				±800 ±600	/ +25-30				/ -0.05(20K)
[53]	LSMO/STO	0.5-1 50-100						3×10^{-2} 3×10^{-3}	0.78		
[54]	LSMO/ STO-based LSMO/ BTO-based		330 350	320 350	10 0		25(10K)				
[19]	LSMO:ZnO										-20
[49]	LSMO:ZnO (VAN)										37 (110 K)

To go further in the analysis of the LFMR, at very low magnetic field (less than 0.5 T) a butterfly shape can be observed in figure 6. The different crystalline orientations of the individual grains lead to a misalignment of the spin directions, dominated by the local orientation of the magnetic easy-axis. When the field is enhanced, the magnetization of the individual grains will align progressively with the external magnetic field, and the mobile charges can move more easily form one grain to the other, reducing the electrical resistance. The butterfly shape is related to the magnetization rotation of the grains and their magnetic hysteresis (see figure S5). This relationship is well visible in figure 6 by the comparison of the magnetoresistance and the hysteresis loops from magnetic measurements obtained for the same sample.

Furthermore, the CSE approach allows to use extremely thin LSMO layer, subject to shape anisotropy favoring the in-plane orientation of the spins. This shape anisotropy is well observed in the CSE films (figure 6a and b) leading to an easy-axis type magnetic hysteresis in the plane of the sample, and to a hard-axis type hysteresis perpendicular to the plane [13,17,18,38,55–59]. This change in magnetic reorientation of the grains has also its influence on the MR of butterfly effect: the amplitude is higher for the in-plane direction, with narrow peaks reflecting a strong sensitivity to the magnetic field, and the positioning of the peaks at low fields. The MR properties of the CSE films are therefore not isotropic as they would be in thicker polycrystalline films, and they depend on the direction of the applied field. This effect may be interesting for the development of oriented magnetic sensors [60], allowing to determine not only the strength of the measured magnetic field, but also its orientation with respect to the sensor.

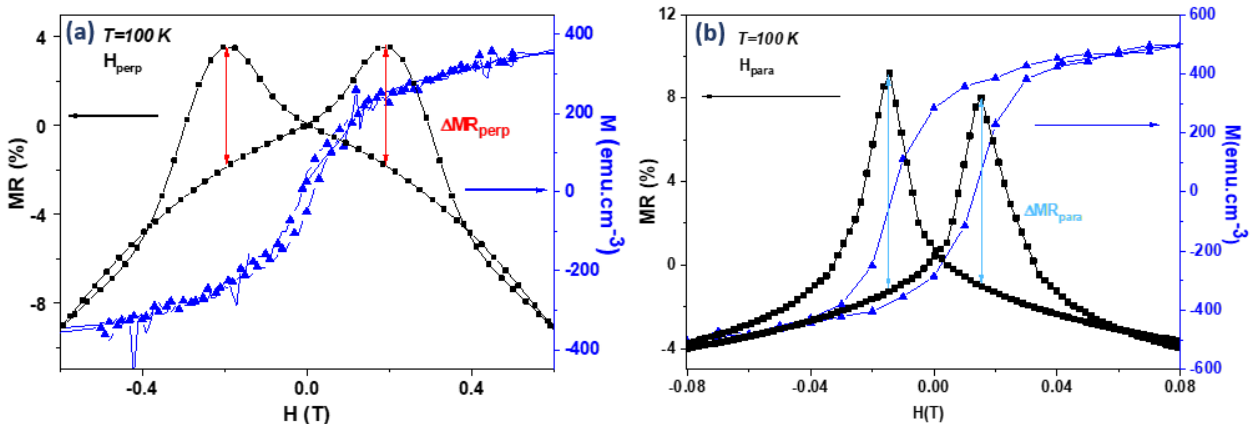

Figure 6. Representative plot, measured at 100 K, of MR and magnetization, for LSMO films with 2 µm grains size, as a function of applied magnetic field: perpendicular (a) and parallel (b).

Finally, to evaluate the temperature dependence of this specific MR in the 2 µm sample, the variations were extracted (see figure 7) for the perpendicular (and the parallel field configuration. The ΔMR corresponds to the difference of the MR in the two different branches (increasing and decreasing field) at the temperature-depending MR maximum, as indicated in

figure 6, capturing a large part of the MR in butterfly effect. For both configurations, the decrease of ΔMR are similar with temperature and is still visible until 325 K. To our knowledge, these values of MR obtained by the CSE approach are the more important values reported in the literature [13].

Since this butterfly effect is not present in single-crystal films, this effect may come from two possible contributions due to the polycristalline nature of the CSE films. The first one can be related to a spin-dependent tunneling through grain boundaries as for the LFMR. Nevertheless, since the LFMR is present only up to 230 K, this mechanism can be ruled out. The other possible contribution is an intergrain effect, where the decrease of the grain size will change the magnetic domains during the magnetic switching and enhanced electronic scattering. This is in perfect adequation with high T_C of our film around 350 K.

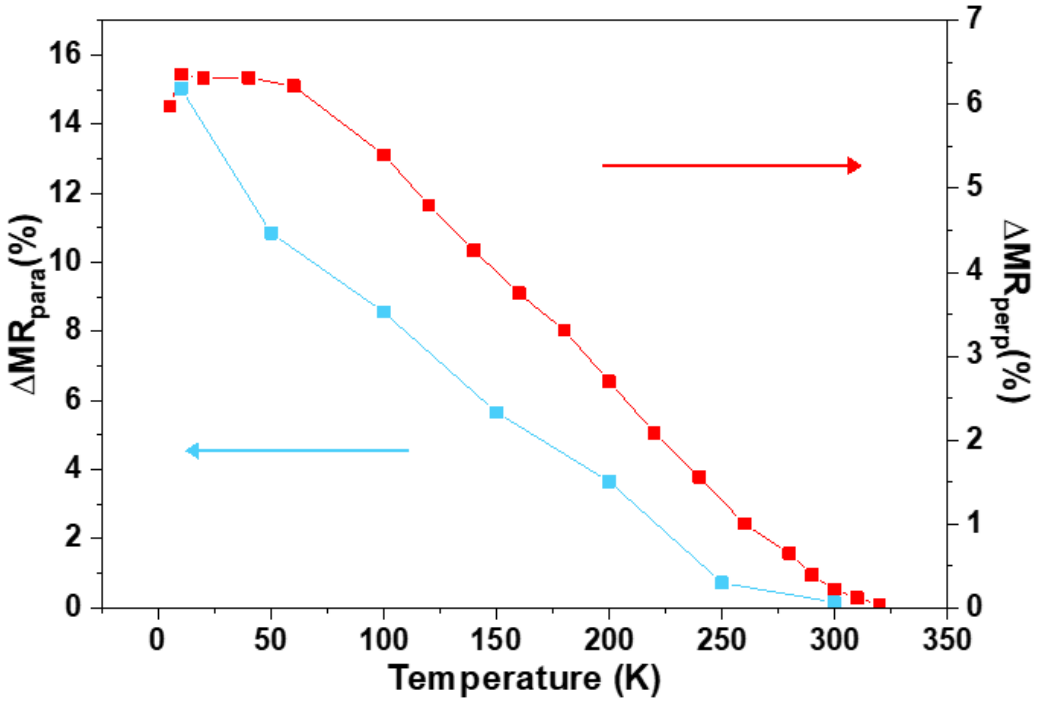

Figure 7. Maximum magnetoresistance of the LSMO film with grain size of 2 µm measured with magnetic field applied perpendicular (red square) and parallel (blue square) to the surface.

4. Conclusions

In summary, LSMO thin films were deposited by using PLD technique on polycrystalline substrates using the CSE approach for grain-in-grain epitaxial growth. As the size of the crystallographic domains can be controlled from 2 to 45 µm during the substrate preparation, we studied the influence of the polycrystalline character and the density of grain boundaries on the magneto-transport properties of LSMO thin films. This approach leads to the presence of a substantial LFMR effect at temperatures below 230 K. Moreover, we demonstrate that the LFMR

effect is enhanced by decreasing the size of the crystalline domains in LSMO films imposed by the control of the grain size in $SrTiO_3$ substrates. Furthermore, a large anisotropy of the MR is observed with respect to the applied field direction due to the magnetic shape anisotropy and the butterfly effect persists up to room temperature. This work demonstrates that we are able to enhance and control the magneto-transport properties of LSMO thin films by the CSE approach, showing a high tunability of the grain sizes in the thin films with equivalent magnetic properties. Thereby, the CSE approach opens new perspectives for manganite oxides. Various applications for functional oxides in electronic or spintronic such as high-resolution low field magnetic sensors are conceivable.

Supporting Information

AFM and EBSD images, determination of Curie temperature, transport properties, magnetization properties.

Conflict of interest

The authors declare that they have no known competing financial interests that could have appeared to influence the work reported in this paper.

Acknowledgements

The authors thank regional funding RIN Doctorants and french agence nationale de la recherche (ANR) (ANR-17-CE08-0012) in the framework of the POLYNASH project. The authors thank J. Lecourt and F.Veillon respectively for substrate preparation and physical measurements.

References

[1] Gariglio S and Triscone J-M 2011 Oxide interface superconductivity *Comptes Rendus Physique* 12 591–9

[2] Tholence J-L and Raveau B 1987 Experiments show the way *Nature* 327 658–9

[3] Tranquada J M, Sternlieb B J, Axe J D, Nakamura Y and Uchida S 1995 Evidence for stripe correlations of spins and holes in copper oxide superconductors *Nature* 375 561–3

[4] Bowen M, Bibes M, Barthélémy A, Contour J-P, Anane A, Lemaître Y and Fert A 2003 Nearly total spin polarization in La2/3Sr1/3MnO3 from tunneling experiments *Appl. Phys. Lett.* 82 233–5

[5] Bibes M, Villegas J E and Barthélémy A 2011 Ultrathin oxide films and interfaces for electronics and spintronics *Advances in Physics* 60 5–84

[6] Xu Y, Memmert U and Hartmann U 2001 Magnetic field sensors from polycrystalline manganites *Sensors and Actuators A: Physical* 91 26–9

[7] Huang J, Wang H, Sun X, Zhang X and Wang H 2018 Multifunctional La $_{0.67}$ Sr $_{0.33}$ MnO $_{3}$ (LSMO) Thin Films Integrated on Mica Substrates toward Flexible Spintronics and Electronics *ACS Appl. Mater. Interfaces* 10 42698–705

[8] Haghiri-Gosnet A-M and Renard J-P 2003 CMR manganites: physics, thin films and devices *J. Phys. D: Appl. Phys.* 36 R127–50

[9] Coey J M D, Viret M, Ranno L and Ounadjela K 1995 Electron Localization in Mixed-Valence Manganites *Phys. Rev. Lett.* 75 3910–3

[10] Fontcuberta J, Martínez B, Seffar A, Piñol S, García-Muñoz J L and Obradors X 1996 Colossal Magnetoresistance of Ferromagnetic Manganites: Structural Tuning and Mechanisms *Phys. Rev. Lett.* 76 1122–5

[11] Murugavel P, Padhan P and Prellier W 2006 Effect of oxygen pressure on the interface related magnetic and transport properties of La $_{0.7}$ Sr $_{0.3}$ MnO $_{3}$ /BaTiO $_{3}$ superlattices *J. Phys.: Condens. Matter* 18 3377–84

[12] Ramirez A P Colossal magnetoresistance *Journal of physics. Condensed matter (Print). 9(39):8171-8199* 30

[13] Bibes M, Martínez B, Fontcuberta J, Trtik V, Benítez F, Sánchez F and Varela M 1999 Laser patterned arrays of interfaces in magnetoresistive La2/3Sr1/3MnO3 thin films *Appl. Phys. Lett.* 75 2120–2

[14] Navin K and Kurchania R 2018 Structural, magnetic and transport properties of the La 0.7 Sr 0.3 MnO 3 -ZnO nanocomposites *Journal of Magnetism and Magnetic Materials* 448 228–35

[15] Li J, Wang P, Xiang J Y, Zhu X H, Peng W, Chen Y F, Zheng D N and Li Z W 2005 Large low-field magnetoresistance observed in twinned La2⁄3Ca1⁄3MnO3 thin films epitaxially grown on yttria-stabilized zirconia-buffered silicon on insulator substrates *Appl. Phys. Lett.* 86 112514

[16] Fadil D, Wu S, Perna P, Renault B, Saïb M, Lebargy S, Gasnier J, Guillet B, Routoure J-M, Flament S and Méchin L 2012 Direct observation of magnetization reversal and low field magnetoresistance of epitaxial La $_{0.7}$ Sr $_{0.3}$ MnO $_{3}$ /SrTiO $_{3}$ (001) thin films at room temperature *Journal of Applied Physics* 112 013906

[17] Balcells L, Carrillo A E and Mart B 2000 Room temperature magnetoresistive sensor based on thick "lms manganese perovskite *Journal of Magnetism and Magnetic Materials* 7

[18] Li X W, Gupta A, Xiao G and Gong G Q 1997 Low-field magnetoresistive properties of polycrystalline and epitaxial perovskite manganite films *Appl. Phys. Lett.* 71 1124–6

[19] Staruch M, Gao H, Gao P-X and Jain M 2012 Low-Field Magnetoresistance in La0.67Sr0.33MnO3:ZnO Composite Film *Adv. Funct. Mater.* 22 3591–5

[20] Sun X, Li Q, Huang J, Jian J, Lu P, Zhang X, MacManus-Driscoll J L and Wang H 2019 Strain and property tuning of the 3D framed epitaxial nanocomposite thin films via interlayer thickness variation *Journal of Applied Physics* 125 082530

[21] Lacotte M, David A, Pravarthana D, Grygiel C, Rohrer G S, Salvador P A, Velazquez M, de Kloe R and Prellier W 2014 Growth of Ca_2MnO_4 Ruddlesden-Popper structured thin films using combinatorial substrate epitaxy *Journal of Applied Physics* 116 245303

[22] Pravarthana D, Lebedev O I, Hebert S, Chateigner D, Salvador P A and Prellier W 2013 High-throughput synthesis of thermoelectric $Ca_3Co_4O_9$ films *Appl. Phys. Lett.* 103 143123

[23] Pravarthana D, Chateigner D, Lutterotti L, Lacotte M, Marinel S, Dubos P A, Hervas I, Hug E, Salvador P A and Prellier W 2013 Growth and texture of spark plasma sintered Al_2O_3 ceramics: A combined analysis of X-rays and electron back scatter diffraction *Journal of Applied Physics* 113 153510

[24] Pravarthana D, Trassin M, Haw Chu J, Lacotte M, David A, Ramesh R, Salvador P A and Prellier W 2014 $BiFeO_3$ /$La_{0.7}Sr_{0.3}MnO_3$ heterostructures deposited on spark plasma sintered $LaAlO_3$ substrates *Appl. Phys. Lett.* 104 082914

[25] Woo S, Jeong H, Lee S A, Seo H, Lacotte M, David A, Kim H Y, Prellier W, Kim Y and Choi W S 2015 Surface properties of atomically flat poly-crystalline SrTiO3 *Sci Rep* 5 8822

[26] Pravarthana D, Lebedev O I, David A, Fouchet A, Trassin M, Rohrer G S, Salvador P A and Prellier W 2019 Metastable monoclinic [110] layered perovskite $Dy_2Ti_2O_7$ thin films for ferroelectric applications *RSC Adv.* 9 19895–904

[27] Lacotte M, David A, Rohrer G S, Salvador P A and Prellier W 2015 Preferential orientation relationships in Ca2MnO4 Ruddlesden-Popper thin films *Journal of Applied Physics* 118 045306

[28] Woo S, Lee S A, Mun H, Choi Y G, Zhung C J, Shin S, Lacotte M, David A, Prellier W, Park T, Kang W N, Lee J S, Kim S W and Choi W S 2018 Enhanced magnetic and thermoelectric properties in epitaxial polycrystalline SrRuO3 thin films *Nanoscale* 10 4377–84

[29] Sadoc A, Mercey B, Simon C, Grebille D, Prellier W and Lepetit M-B 2010 Large Increase of the Curie Temperature by Orbital Ordering Control *Phys. Rev. Lett.* 104 046804

[30] Mercey B, David A, Copie O and Prellier W 2016 Monitoring the growth of SrTiO3 and La0.66Sr0.33MnO3 thin films using a low-pressure Reflection High Energy Electron Diffraction system *Physica B: Condensed Matter* 503 100–5

[31] Brivio S, Cantoni M, Petti D, Cattoni A, Bertacco R, Finazzi M, Ciccacci F, Sidorenko A, Allodi G, Ghidini M and de Renzi R 2007 Decrease of the Curie temperature in La0.67Sr0.33MnO3 thin films induced by Au capping *Materials Science and Engineering: B* 144 93–6

[32] Ziese M 2002 Extrinsic magnetotransport phenomena in ferromagnetic oxides *Rep. Prog. Phys.* 65 143–249

[33] Anon Kwon, C.; Robson, M. C.; Kim, K.-C.; Gu, J. Y.; Lofland, S. E.; Bhagat, S. M.; Trajanovic, Z.; Rajeswari, M.; Venkatesan, T.; Kratz, A. R. Stress-induced Effects in Epitaxial (La0.7Sr0.3)MnO3 Films. Journal of magnetism and magnetic materials 1997, 172 (3), 229–236.

[34] Boileau A, Dallocchio M, Baudouin F, David A, Lüders U, Mercey B, Pautrat A, Demange V, Guilloux-Viry M, Prellier W and Fouchet A 2019 Textured Manganite Films Anywhere *ACS Appl. Mater. Interfaces* 11 37302–12

[35] Tsui F, Smoak M C, Nath T K and Eom C B 2000 Strain-dependent magnetic phase diagram of epitaxial La0.67Sr0.33MnO3 thin films *Appl. Phys. Lett.* 76 2421–3

[36] Siwach P K, Singh H K and Srivastava O N 2008 Low field magnetotransport in manganites *J. Phys.: Condens. Matter* 20 273201

[37] Yang S Y, Kuang W L, Liou Y, Tse W S, Lee S F and Yao Y D 2004 Growth and characterization of La0.7Sr0.3MnO3 films on various substrates *Journal of Magnetism and Magnetic Materials* 268 326–31

[38] Hwang H Y, Cheong S-W, Ong N P and Batlogg B 1996 Spin-Polarized Intergrain Tunneling in La 2 / 3 Sr 1 / 3 MnO 3 *Phys. Rev. Lett.* 77 2041–4

[39] Chopdekar R V, Arenholz E and Suzuki Y 2009 Orientation and thickness dependence of magnetization at the interfaces of highly spin-polarized manganite thin films *Phys. Rev. B* 79 104417

[40] Chaluvadi S K, Ajejas F, Orgiani P, Lebargy S, Minj A, Flament S, Camarero J, Perna P and Méchin L 2020 Epitaxial strain and thickness dependent structural, electrical and magnetic properties of $La_{0.67}Sr_{0.33}MnO_3$ films *J. Phys. D: Appl. Phys.* 53 375005

[41] Dey P, Nath T K and Taraphder A 2007 Effect of substrate-induced strain on transport and magnetic properties of epitaxial La0.66Sr0.33MnO3 thin films *Appl. Phys. Lett.* 91 012511

[42] Gupta A, Gong G Q, Xiao G, Duncombe P R, Lecoeur P, Trouilloud P, Wang Y Y, Dravid V P and Sun J Z 1996 Grain-boundary effects on the magnetoresistance properties of perovskite manganite films *Phys. Rev. B* 54 R15629–32

[43] Haghiri-Gosnet A M, Wolfman J, Mercey B, Simon C, Lecoeur P, Korzenski M, Hervieu M, Desfeux R and Baldinozzi G 2000 Microstructure and magnetic properties of strained La0.7Sr0.3MnO3 thin films *Journal of Applied Physics* 88 4257

[44] Gupta S, Ranjit R, Mitra C, Raychaudhuri P and Pinto R 2001 Enhanced room-temperature magnetoresistance in La0.7Sr0.3MnO3-glass composites *Appl. Phys. Lett.* 78 362–4

[45] Chen A, Bi Z, Hazariwala H, Zhang X, Su Q, Chen L, Jia Q, MacManus-Driscoll J L and Wang H 2011 Microstructure, magnetic, and low-field magnetotransport properties of self-assembled $(La_{0.7}Sr_{0.3}MnO_3)_{0.5}$:$(CeO_2)_{0.5}$ vertically aligned nanocomposite thin films *Nanotechnology* 22 315712

[46] Zhang W, Li L, Lu P, Fan M, Su Q, Khatkhatay F, Chen A, Jia Q, Zhang X, MacManus-Driscoll J L and Wang H 2015 Perpendicular Exchange-Biased Magnetotransport at the Vertical Heterointerfaces in $La_{0.7}Sr_{0.3}MnO_3$:NiO Nanocomposites *ACS Appl. Mater. Interfaces* 7 21646–51

[47] Chen A, Bi Z, Tsai C-F, Lee J, Su Q, Zhang X, Jia Q, MacManus-Driscoll J L and Wang H 2011 Tunable Low-Field Magnetoresistance in (La0.7Sr0.3MnO3)0.5:(ZnO)0.5 Self-Assembled Vertically Aligned Nanocomposite Thin Films *Adv. Funct. Mater.* 21 2423–9

[48] Kang B S, Wang H, MacManus-Driscoll J L, Li Y, Jia Q X, Mihut I and Betts J B 2006 Low field magnetotransport properties of (La0.7Sr0.3MnO3)0.5:(ZnO)0.5 nanocomposite films *Appl. Phys. Lett.* 88 192514

[49] Sun X, Kalaswad M, Li Q, Paldi R L, Huang J, Wang H, Gao X, Zhang X and Wang H 2020 Role of Interlayer in 3D Vertically Aligned Nanocomposite Frameworks with Tunable Magnetotransport Properties *Adv. Mater. Interfaces* 1901990

[50] Raychaudhuri P, Sheshadri K, Taneja P, Bandyopadhyay S, Ayyub P, Nigam A K, Pinto R, Chaudhary S and Roy S B 1999 Spin-polarized tunneling in the half-metallic ferromagnets La 0.7 − x Ho x Sr 0.3 MnO 3 (x = 0 and 0.15): Experiment and theory *Phys. Rev. B* 59 13919–26

[51] Zhang N, Ding W, Zhong W, Xing D and Du Y Interfacial tunnel-type GMR in granular perovskite La-Sr-Mn-O system 5

[52] Romero M, Faccio R, Pardo H, Tumelero M A, Montenegro B, Campos Plá Cid C, Pasa A A and Mombrú Á W 2015 The effect of manganite nanoparticle addition on the low field magnetoresistance of polyaniline *J. Mater. Chem. C* 3 12040–7

[53] Balcells L L, Fontcuberta J, Martínez B and Obradors X 1998 Magnetic surface effects and low-temperature magnetoresistance in manganese perovskites *J. Phys.: Condens. Matter* 10 1883–90

[54] Perna P, Méchin L, Chauvat M P, Ruterana P, Simon C and Scotti di Uccio U 2009 High Curie temperature for La $_{0.7}$ Sr $_{0.3}$ MnO $_{3}$ thin films deposited on CeO $_{2}$ /YSZ-based buffered silicon substrates *J. Phys.: Condens. Matter* 21 306005

[55] Ju H L, Gopalakrishnan J, Peng J L, Li Q, Xiong G C, Venkatesan T and Greene R L 1995 Dependence of giant magnetoresistance on oxygen stoichiometry and magnetization in polycrystalline La 0.67 Ba 0.33 MnO z *Phys. Rev. B* 51 6143–6

[56] Dieny B, Speriosu V S, Parkin S S P, Gurney B A, Wilhoit D R and Mauri D 1991 Giant magnetoresistive in soft ferromagnetic multilayers *Phys. Rev. B* 43 1297–300

[57] Gupta A, Li X W and Xiao G 2000 Magnetic and transport properties of epitaxial and polycrystalline chromium dioxide thin films (invited) *Journal of Applied Physics* 87 6073–8

[58] Coey J M D, Berkowitz A E, Balcells Ll, Putris F F and Barry A 1998 Magnetoresistance of Chromium Dioxide Powder Compacts *Physical Review Letters* 80 3815–8

[59] Klein L, Dodge J S, Ahn C H, Reiner J W, Mieville L, Geballe T H, Beasley M R and Kapitulnik A 1996 Transport and magnetization in the badly metallic itinerant ferromagnet *J. Phys.: Condens. Matter* 8 10111–26

[60] Perna P, Maccariello D, Ajejas F, Guerrero R, Méchin L, Flament S, Santamaria J, Miranda R and Camarero J 2017 Engineering Large Anisotropic Magnetoresistance in La $_{0.7}$ Sr $_{0.3}$ MnO $_{3}$ Films at Room Temperature *Advanced Functional Materials* 27 1700664

For Table of Contents only: